Design, Assembly, Calibration, and Measurement of an Augmented Reality Haploscope

Nate Phillips* Mississippi State University
Kristen Massey† Mississippi State University
Mohammed Safayet Arefin‡ Mississippi State University
J. Edward Swan II§ Mississippi State University

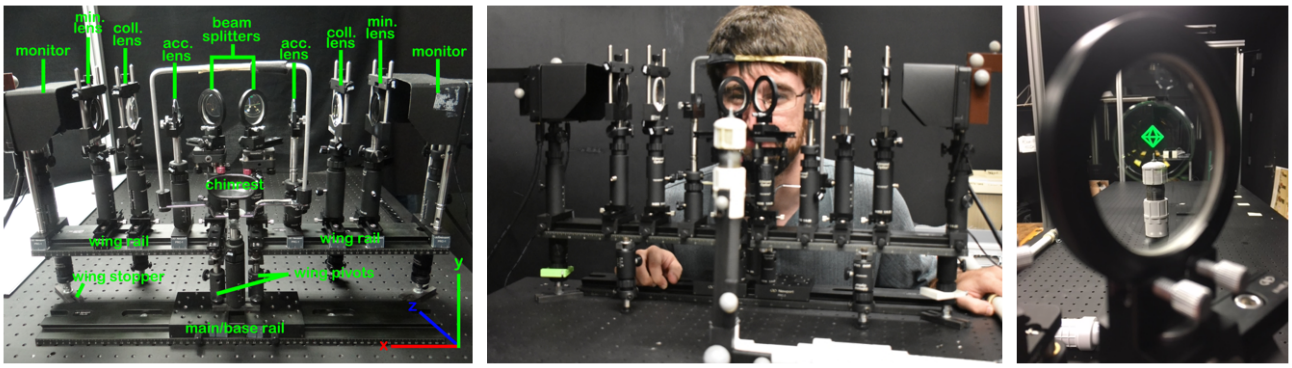

Figure 1: The Augmented Reality (AR) haploscope. (a) A front view of the AR haploscope with labeled components [11]. (b) A user participating in perceptual experiments. (c) The user's view through the haploscope. With finely adjusted parameters such as brightness, binocular parallax, and focal demand, this object appears to have a definite spatial location.

Abstract

A haploscope is an optical system which produces a carefully controlled virtual image. Since the development of Wheatstone's original stereoscope in 1838, haploscopes have been used to measure perceptual properties of human stereoscopic vision. This paper presents an augmented reality (AR) haploscope, which allows the viewing of virtual objects superimposed against the real world. Our lab has used generations of this device to make a careful series of perceptual measurements of AR phenomena, which have been described in publications over the previous 8 years. This paper systematically describes the design, assembly, calibration, and measurement of our AR haploscope. These methods have been developed and improved in our lab over the past 10 years. Despite the fact that 180 years have elapsed since the original report of Wheatstone's stereoscope, we have not previously found a paper that describes these kinds of details.

1 Introduction

Mixed reality has been an active field of research for the past 50 years [18], but recent advances and interest have dramatically accelerated developments in the field. This has resulted, lately, in an explosive increase in the development of virtual and augmented reality (AR) display devices, such as the Vuzix STAR, Oculus Rift, Google Glass, Microsoft HoloLens, HTC Vive, Meta 2, and Magic Leap One. These displays have inspired consumer and business interest, increased demand for VR and AR applications, and motivated increased investment in VR and AR development and research [13].

*e-mail: Nathaniel.C.Phillips@ieee.org
†e-mail: kristenmassey@ieee.org
‡e-mail:arefin@acm.org
§e-mail: swan@acm.org

This is an author version preprint. The final version is available as: Nate Phillips, Kristen Massey, Mohammed Safayet Arefin, J. Edward Swan II, "Design, Assembly, Calibration, and Measurement of an Augmented Reality Haploscope", *Proceedings of PERCAR: The Fifth IEEE VR Workshop on Perceptual and Cognitive Issues in AR, 2019 IEEE Conference on Virtual Reality and 3D User Interfaces*, Osaka, Japan, March 23–27, pages 1770–1774, 2019. DOI: 10.1109/VR.2019.8798335, preprint: arXiv:1908.08532.

This investment and development is stymied by an incomplete knowledge of key underlying research. Among this unfinished research, our lab has focused on addressing questions of AR perception; in order to accomplish the ambitious goals of business and industry, a deeper understanding of the perceptual phenomena underlying AR is needed [9]. All current commercial AR displays have certain limitations, including fixed focal distances, limited fields of view, non-adjustable optical designs, and limited luminance ranges, among others. These limitations hinder the ability of our field to ask certain research questions, especially in the area of AR perception.

Therefore, our lab has developed a custom AR display (Figure 1), which we call the *AR Haploscope*, and which we assembled from off-the-shelf optical components. Our design, iterated through several generations and research projects ([2, 7, 14–17]), is based on previous haploscope research (e.g., [3, 23]), which has been widely used in the field of visual perception [21]. A *haploscope* is an optical system that produces tightly-controlled virtual images, typically with controlled accommodative demand, presented angle, brightness, divergence, and image choice [2, 7, 15]. Such a system is completely controllable, can be adjusted for different inter-pupillary distances, can be set up for a wide range of experiments, and can be reliably re-used. These are some of the features that make haploscopes excellent research tools.

The advantages of using a haploscope come with the additional burden of calibration. Through our own experience, we have discovered that the calibration of an AR haploscope is a non-trivial task. There are several important factors to consider and compensate for, as well as many potential pitfalls [12]. The difficulty is compounded by a general dearth of published research on the topic of haploscope calibration; the authors have looked for, but not found, such a publication.

Therefore, this paper seeks to contribute a systematic description and evaluation of the design, assembly, and calibration of an AR haploscope system.

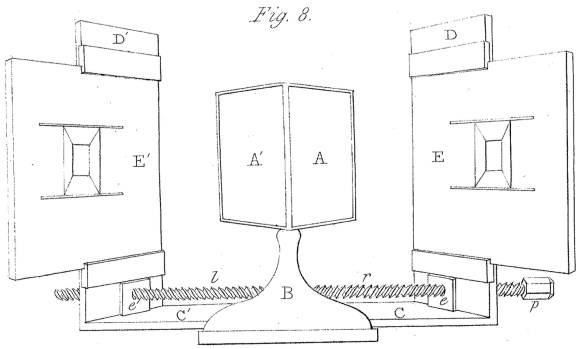

Figure 2: The *stereoscope*, from Wheatstone [22, Figure 8]. Panels D' and D hold drawings E' and E, which are reflected by mirrors A' and A, into the observer's eyes. The mirrors are mounted 90° from each other, and 45° from the optic axis. The stereoscope makes it easy for most observers to stereo fuse E' and E. This design forms the basis of most haploscopes.

2 Background

Since the discovery of perspective in the 14th century by Italian Renaissance painters and architects, scholars and scientists have been studying human stereo vision. In 1838, Wheatstone [22] gave the first scientific description of the phenomena of stereopsis. He also described the *stereoscope* (Figure 2)—the seminal instrument for precisely displaying a stereo pair of images. A haploscope is fundamentally a stereoscope that has been adapted for laboratory use.

Historically, haploscopes are instruments that are used to observe stereo vision and measure accommodation, vergence, and other properties of human eyes, across many disparate research fields. In 1959, Williams [23] designed and developed a haploscope in the physiologic optics laboratory. Williams' haploscope had the capability to independently control the stimulus to accommodation and convergence. As part of the NASA Vision testing system (NVTS) [3], NASA developed the Baylor Mark III Haploscope to measure, record and analyze the binocular vision of astronauts during spaceflight. Ellis et al. [6], in 1994, produced a novel head-mounted haploscope system to study the effects of interposition and occlusion on virtual images. Finally, Rolland et al. [12] developed and used their own haploscope in order to study the accuracy and precision of depth judgments. These examples represent only a small sampling of historical haploscope usage, but are largely representative of haploscopes in research.

In augmented reality in particular, haploscopes are useful for investigating topics like IPD mismatch, accommodation-vergence mismatch, depth perception, and various other important research areas. In order to analyze near field depth perception in AR, Singh designed and built a haploscope with dynamic focus adjustment and rotatable optics [14]. Later, this haploscope setup was used to make additional measurements [15, 19]. Another haploscope system was created by Banks et al. [1]; it was used to examine binocular disparity and eye-position. In addition, Domini [5, 20] created a haploscope setup in order to analyze vergence angle effects.

3 Haploscope Design

A haploscope is an augmented reality tabletop apparatus that presents images to users through a lens system (Figure 1). Our particular haploscope, which is based on Singh's design [14, 16], presents an image and then collimates it. After collimation, the *accommodation lens* forms an image at any arbitrary distance. This apparatus also allows free rotation about the modeled eye position of the user, allowing *alpha*, sometimes also called the vergence angle or angle

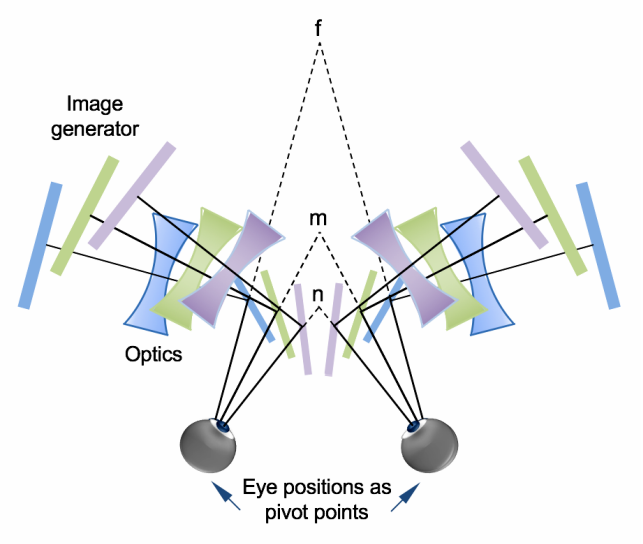

Figure 3: An example of how the haploscope wings rotate to match different focal distances, from Singh [14, Figure 4.7]. The displays rotate inward as a user's eyes rotate, ensuring that the user maintains a view fixed at the optical center where distortion is minimized.

of binocular parallax, to be readily adjusted without adding any additional optical distortion [16].

It may be instructive to examine the workings of the haploscope, outlined in brief above, in slightly more detail (Figure 5). At the start, the haploscope monitor generates an image source. Then, that image is shrunk by the *minimization lens*, a -10 diopter concave lens, producing a minified virtual image 5 cm in front of the lens. This minified image, in turn, is collimated by the *collimating lens*, a 10 diopter convex lens, positioned 10 cm in front of the minified image. Now, collimated light, definitionally, is broadcast out in purely parallel rays of light, formed at optical infinity. Once the collimated image source nears the user's eye, it is focused, by application of a particular negative power concave lens, to the particular focal distance desired. The power of these lenses' range from 0 diopters, which simply passes the collimated image through, all the way up to 20 diopters, well beyond a normal user's focal ability. Finally, the output of this lens system is reflected into a user's eye by a *beamsplitter*, a partially reflective piece of glass. This beamsplitter allows the user to see both the reflected virtual object and the real world displayed beyond the beamsplitter [16].

However, even this is not enough to fully control all the cues that a user needs to perceive an object. Most notably, users also need to be able to converge appropriately to the visual target. During vergence, a user's eyes rotate inward or outward so that they can center the viewed object in their vision. For objects at a specific distance, this effect causes the eyes to rotate to a particular angle, α, cumulatively called the vergence angle or angle of binocular parallax (Figure 4), which can be readily calculated by the formula:

$$\alpha = \arctan \frac{\text{object distance}}{(\text{IPD}/2)}, \tag{1}$$

where IPD is the user's interpupillary distance.

As such, this haploscope design needs to be able to accurately and precisely rotate to a variety of vergence angles. With a non-rotating haploscope, there is a significant problem with this; as the user eye rotates, the haploscope is not able to rotate with it and so the user is presented with images suffering from increasing levels of optical distortion [14]. With a haploscope, like ours, that rotates about the

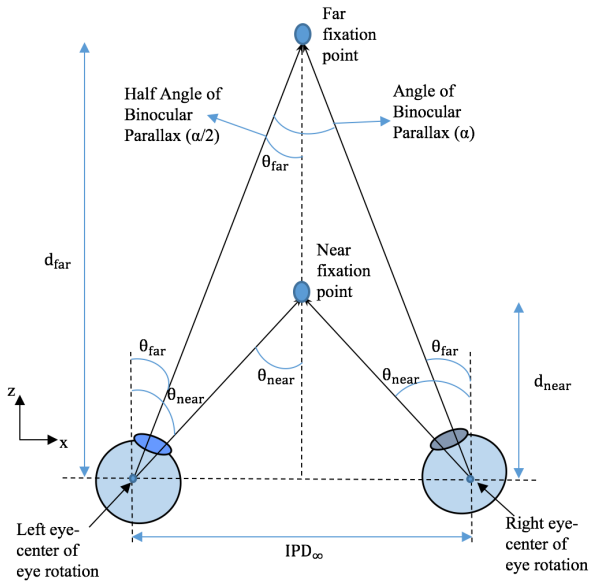

Figure 4: An example eye model of the haploscope. As a user fixates at different distances, his or her eyes rotate about the center of rotation.

modeled eye position, the system's optical axes can be rotated to be collinear with the user's optical axes, eliminating this additional distortion (Figure 3).

Thus, this haploscope system controls many of the perceptual cues necessary to perceive an object. Several less notable cues that we can control, but that have not been discussed so far include: brightness, color, and shape, which can be easily adjusted through the LCD screen or supporting code; dipvergence, or vertical misalignment of the stereo images, which can be controlled by adjusting the height of the LCD images relative to each other; movement, controlled by the program driving the monitors; and occlusion, which can be controlled by the placement of physical objects in the environment and by manually adjusting the program driving the LCD screens. Each of these factors is, arguably, quite important to depth perception, but, overall, relatively trivial in implementation.

At this point, it may be instructive to briefly discuss our assumptions about human vision (Figure 6). We assume that a human eye can be accurately modeled as a simple schematic eye with a center of rotation, a single nodal point, and a pupil, all of which are colinear with each other [8, 21]. This means, in practice, that human vision takes place on the axis that includes the pupil, the nodal point (from whence human visual perception originates), and the center of eye rotation. This model turns out to be rather important, as it has particularly key implications for how we set up the haploscope for a given user.

Initially, our approach to setting up the haploscope for a specific user is fairly simple (Figure 4). We measure a user's IPD when they are focused at infinity (which is when the gaze vectors from both eyes are essentially parallel) and then set up the haploscope such that the pivot points are exactly that distance apart. This distance is important primarily because it is how far the center of a user's eyes are from each other; thus, adjusting the haploscope to this position allows us to align the centers of rotation of a user's eyes with the optical system

Since the centers of the user's eyes and the haploscope system's centers of rotation are coincident, the haploscope optical axes remain aligned with the user's optical axes, even as the eyes/haploscope rails rotate (Figure 6). This means that each point on the user's optical axes, including the nodal point, is presented with the same optical stimuli, regardless of rotation. As such, there are no distance or angle anomalies as each side rotates, since both the eye and the haploscope side are definitionally rotating at the same angle. One of the notable advantages of this setup is that the distances between all the elements are constant and so we do not have to worry about such problems as the changing location of the pupil, varying distances between the eye and the optical setup, or potential misalignments [10]. This serves to make our haploscope significantly easier to use and more reliable than other possible haploscope setups, as well as more resilient to optical distortion.

4 Assembly and Calibration

Haploscope calibration can be broken down into multiple, discrete steps, listed here. For a more in-depth examination of each step, please see Massey [11].

1. Ensure that the haploscope rests upon a flat, level surface and that each element of the haploscope is also flat and level. Further, ensure that the two rotating sides of the haploscope are flat, level, and parallel with each other (Figures 7 and 1).

2. Ensure that the monitors, and all optical components besides the beamsplitters, are mounted such that they are centered along the optical axis of their respective rotating component (Figures 8 and 1).

3. Ensure that the collimation and minimization lenses are positioned on the rails such that they collimate the image from the monitor (Figures 5 and 9).

4. Ensure that the beam splitters are centered such that they are directly in front of the pivot points of both rotating components. Further, ensure that the beam splitters are angled, positioned, and tilted so as to ensure that each rotating component's optical axis is reflected through the beamsplitter such that the reflected ray is then parallel to each rail's optical axis and passes through the component pivot point (Figure 11).

5. Adjust the haploscope IPD for each new user. Finally, verify, as much as is possible, that all previously checked conditions remain true (Figure 10).

Note that errors introduced in any step can be compounded in later steps.

4.1 Step 1 - Tabletop Setup

The first steps in building or calibrating an accurate haploscope system are to ensure that the structure the haploscope is built on is rigid and flat, and that it is balanced with respect to gravity (Figure 7).

Next, a gravity-balanced laser level should be set up and adjusted such that it is parallel to the haploscope table (Figure 8). With this laser level and its autobalancing feature, we are able to use the ruled holes on the haploscope table to generate a precise coordinate plane to use as a ground truth during haploscope calibration. This coordinate plane defines an accurate and precise baseline for evaluating haploscope alignment, and so is an important component of calibration.

4.2 Step 2 - Optical Element Mounting

To mount the optical elements to the sides of the haploscope, it is important that they all be centered on their respective rail, and, thus, the corresponding optical axis, and that they be square with respect to the optical axis. To do this, the laser level coordinate system and a simple mounting block are used to align the center of each element with the center of the haploscope rail.

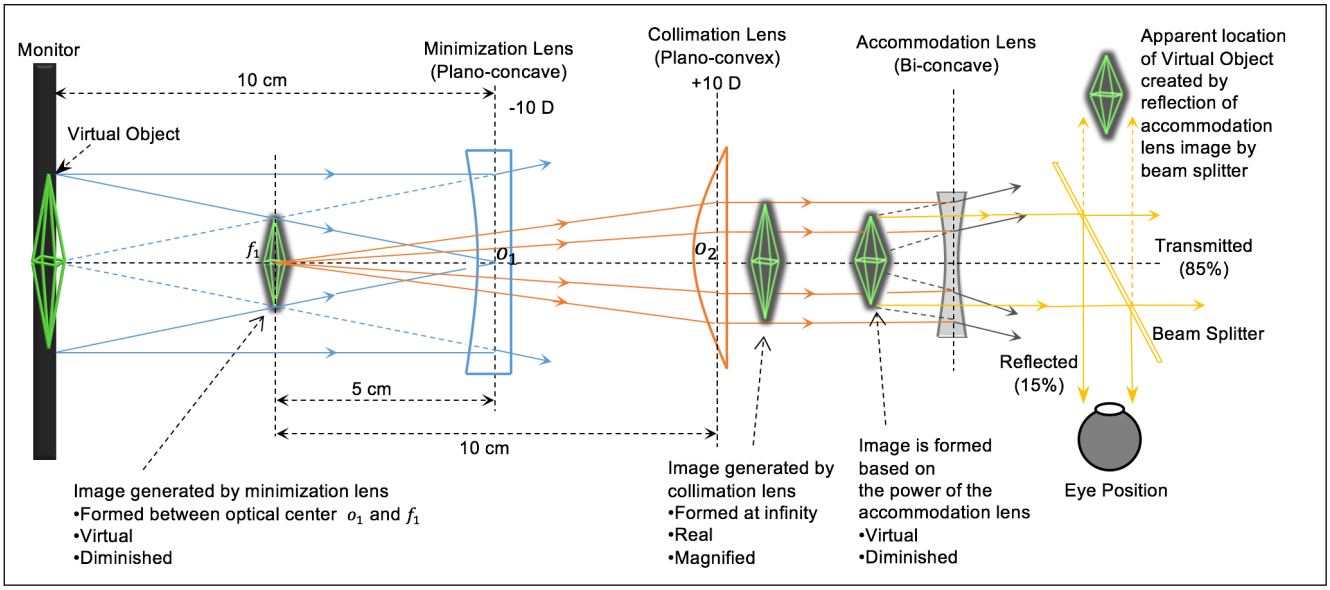

Figure 5: Ray diagram of the side of the haploscope, based on Singh [14, Figure 4.4]. This diagram showcases the path of the virtual object as it is generated by the monitor, shrunk by the minimization lens, collimated by the collimating lens, set to a specific focal distance by the accommodation lens, and finally reflected directly into a user's eye by the beamsplitter.

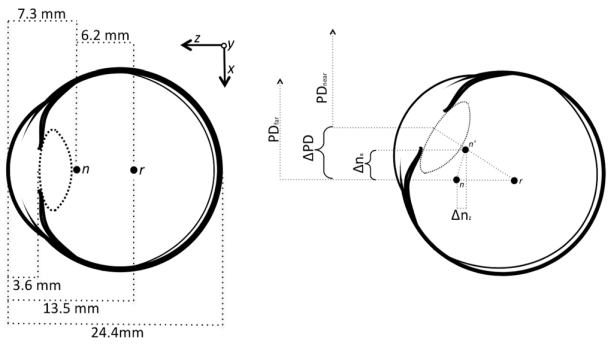

Ocular Feature	Depth	Abbreviation
Corneal Surface	0.0mm	c
Pupil Center	3.6mm	p
Nodal Point	7.3mm	n
Rotational Center	13.5mm	r
Length of Eye	24.4mm	l

Figure 6: Human schematic eye model, from Jones et al. [8, Figure 2]. Note that, with our design, the modeled nodal point of the eye remains equidistant from the optical axis, regardless of haploscope rotation.

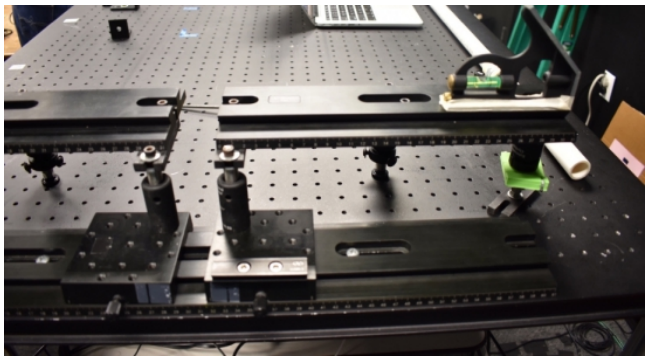

Figure 7: Balancing the haploscope base and both sides of the apparatus is an important first step in calibration. It is also important to ensure that both sides of the haploscope are parallel to each other and that neither side has a forward or backward tilt.

Each rail is rotated outward 90 degrees and securely fastened. The angle of each rail is verified by ensuring that the laser level is shining straight down the center of the rail, as determined by the mounting block center line (Figure 8). Once each side is secured, the monitors are placed on the rail and centered, both vertically and horizontally, by matching the monitor calibration crosshair with the laser level crosshair (Figure 11).

At this point, three known quantities have been established: the laser level defines a coordinate system based on the haploscope table; each optical axis is collinear to this coordinate system; and, finally, the screen crosshair is centered on each rail's optical axis. With these three known quantities, we can create a system to center each optical element individually as we add it to the haploscope. This is done by placing each optical element on the rail, one at a time, and then adjusting its position until the laser crosshair bisects both the element's center and the screen crosshair.

4.3 Step 3 - Collimating the Image Source

Next, it is important that the output from the monitor be collimated; without collimation, it would be untenable to adjust the focal demand of the presented image precisely and accurately, as is required.

To do this, the elements are positioned based on their back focal distance and the well-known thin lens equation,

$$\frac{1}{f} = \frac{1}{u} + \frac{1}{v}, \tag{2}$$

where f represents the focal demand, u represents the object distance,

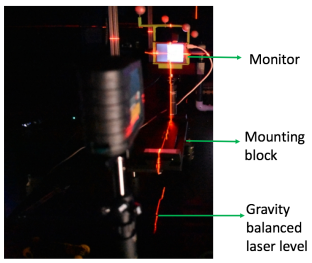

Figure 8: This figure shows a calibrated monitor, appropriately centered and balanced on its side of the haploscope. This ensures that the haploscope presents a virtual image that is centered, clear, and undistorted.

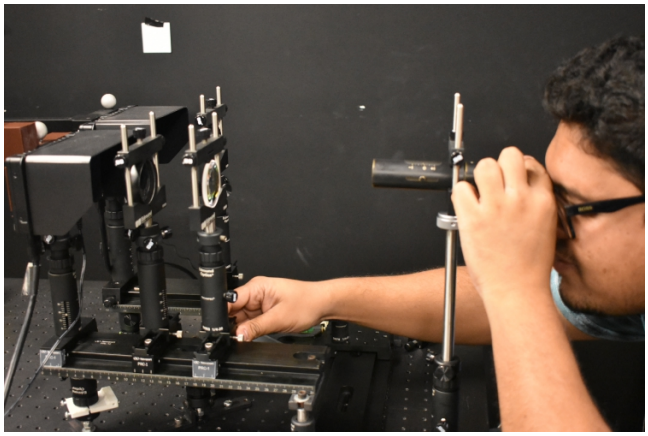

Figure 9: This figure shows an experimenter adjusting the minimization and collimation lenses during dioptometer calibration. This calibration step is important to eliminate focal blur and to verify that the monitor image is appropriately collimated before entering the rest of the lens system.

and v represents the image distance (Figure 5). In essence, the minimization lens, a planoconcave lens, takes the output from the monitor and converts it into a smaller, virtual image. This image is positioned at the planoconvex, or collimating, lens' focal distance and is thus displayed at optical infinity.

To verify that the output of this lens system is correct, we use a dioptometer, a device which allows us to determine if an image is collimated (Figure 9). If the output isn't collimated, we then adjust the position of both lenses until we can verify that their output is indeed collimated.

4.4 Step 4 - Beamsplitter Calibration

At this point, all the remaining optical components should be placed and mounted in their appropriate positions, and the rotating wings returned to infinity vergence (Figure 4).

Next, the beamsplitters must be adjusted until they perfectly match their respective rail's optical axis with a user's modeled optical axis (Figure 5). This requires fine-tuned adjustment of the position, rotation, and tilt/yaw/roll of each beamsplitter. When this calibration step is complete, the laser level defining the coordinate system should be able to connect the modeled eye position and the optical axis for each rail (Figure 11).

Essentially, this calibration step aligns a user's theoretical optical axis with the optical axis of the rail and optical elements. Without this step, the image formed by the beamsplitter could be expected to be highly distorted and misaligned, if it is visible at all; after this

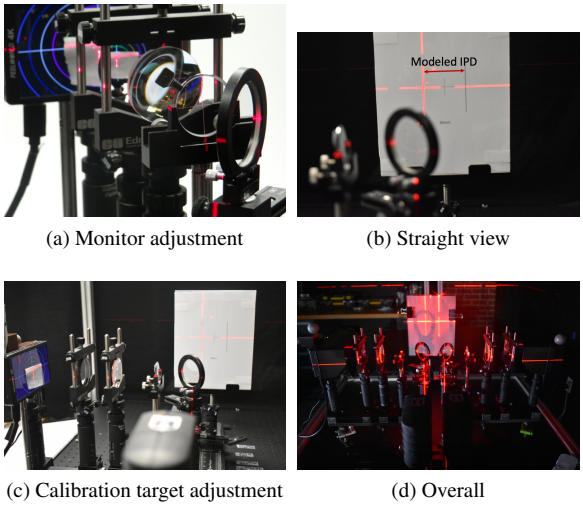

(a) Monitor adjustment (b) Straight view

(c) Calibration target adjustment (d) Overall

Figure 10: IPD Calibration for the left wing, with varying areas in focus: (a) monitor/laser level centering; (b) calibration target centering; (c) an overview of the calibration system; and (d) fully aligned optical axes centered with respect to the calibration target. This alignment verifies that both rails' optical axes are coincident with the optical axes of a user with a given IPD.

step, however, the monitor image should be precisely aligned to the center of the user's visual field.

4.5 Step 5 - IPD Calibration and Verification

The final step in calibrating the haploscope for a specific user is adjusting the system for that user's interpupillary distance (IPD) (Figure 10). If the system is not adjusted based on IPD, the user's optical axis will not be aligned with each rail's optical axis, causing noticeable distortion, angular errors, depth errors, and other problems [10].

One approach to adjusting the system IPD is to set up a calibration target with a displayed distance equal to a potential user's IPD (Figure 10(b)). If two laser levels, separated by the given IPD, can be aligned to either side of the target while also going through the center of each side's optical axis and center of rotation, then the haploscope has been successfully calibrated for that IPD. If not, the base will have to be adjusted until both lasers bisect the calibration target, the appropriate centerline, and their side's center of rotation (Figures 7 and 10(d)).

This methodology also has the notable advantage of verifying the optical element alignment and calibration, which is an important step in guaranteeing an accurate haploscope calibration. The various other calibration steps, where relevant, should also be re-examined to ensure that they still hold true.

5 Evaluation of Angular and Positional Accuracy

At this point, the haploscope system has been calibrated, as completely and effectively as we are currently able. As such, we have found this calibrated system to be useful for perceptual AR research. However, there are some important boundaries on the accuracy of the results produced. Knowing and understanding as many of these error bounds as possible helps to give us a better picture of the haploscope and how best it can be used to test perceptual phenomenon, as well as providing additional engineering challenges similar to those facing traditional AR displays.

Thus, we have devoted significant research time to finding, assessing, and minimizing potential error sources, from the significant to the minuscule, in order to improve our understanding of the haploscope and related perceptual questions and experiments.

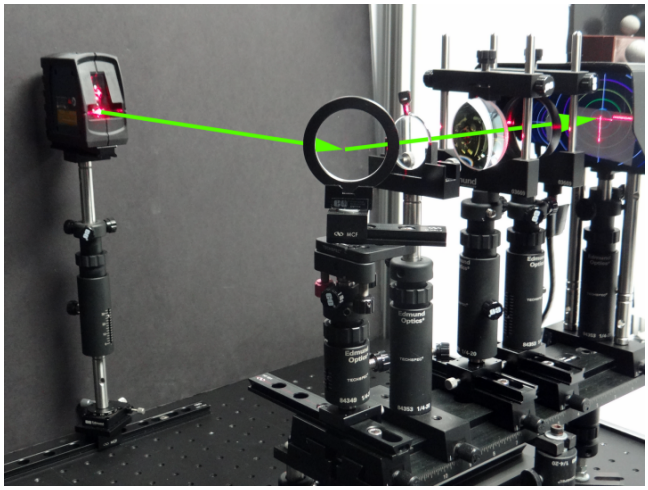

Figure 11: In beamsplitter calibration, the laser level passes through all optical components and rests centered on the monitor crosshairs, reducing optical distortion [11].

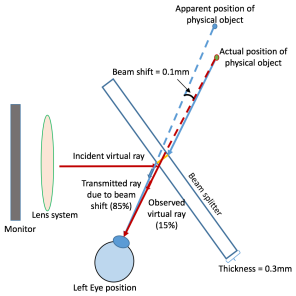

Figure 12: Schematic diagram of the beamshift phenomenon, based on Lee et al. [10, Figure 1]. When the user views the real world through the beamsplitter (the transmitted ray), that view is distorted by the glass, based on Snell's Law.

5.1 Measurement 1: Refraction Error

As seen in Figure 12, one of the primary sources of error in our calibrated haploscope is refraction. As a user focuses outward through the haploscope, his or her view of the real environment is slightly refracted by the beamsplitters, while his or her view of the virtual environment is presented without refraction. As demonstrated by Lee et al. [10], there is a small inward offset in the fixation ray, causing a definite underestimation in distance for a given vergence angle/angle of binocular parallax.

This error, as it turns out, is quite significant, particularly for thick optical combiners. During haploscope use, significant distortion and angular mis-alignments were observed using standard 1.66 mm optical combiners [16]. However, to reduce the severity of this problem, we then switched to very thin 0.3 mm optical combiners. These combiners, while still contributing to refractive error, significantly reduce its impact (Figure 13); in fact, based on a beamsplitter index of refraction of 1.47, Snell's Law indicates that a rayshift of approximately 0.7492 mm can be expected for an optical combiner of thickness 1.66 mm. On the other hand, for an optical combiner of thickness .3 mm, a rayshift of approximately 0.1354 mm can be expected (Figure 13). This, of course, represents a significant improvement over the previous standard, but remains a notable source of error.

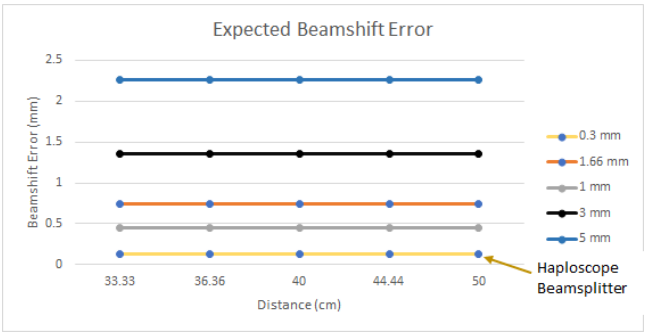

Figure 13: A comparison of the expected beamshift error magnitude with optical combiners of differing thicknesses. Note that the 1, 3, and 5 mm conditions are replicated from Lee et al. [10].

5.2 Measurement 2: Tracker Error

Another potential error source is tracking inaccuracy; when our tracking system measures an angle, by analyzing a constellation of retroreflective markers, the system's results will not be accurate if the measured rotation is inaccurate. As such, we use a simple triangulation system to verify the tracking system's accuracy (Figure 14). In this system, we mount a laser level to one of the haploscope's rotating sides and observe its rotation on a parallel surface 116 cm away. When the side of the haploscope rotates, the distance the laser level travels is measurable and so the error can be calculated through the simple application of trigonometric functions.

To determine the significance and extent of the errors generated by the tracking system, we test the tracking accuracy across thirteen angles, comparing the tracker rotational measurement with the triangulation system previously discussed (Figure 15). These angles, ranging from 1 to 6 degrees, were selected because that range is commonly used in near-field depth perception presentations. Since the triangulation system is measured over a significant distance, most measurement errors that are introduced should be relatively minor. Thus, based on the differences between these two sets of values, we can generate an estimate of the magnitude of the error produced by the tracking system.

5.3 Measurement 3: Vergence Angle Error

One of the more difficult error measures to quantify is the error introduced by experimental inaccuracy. This might include undiscovered errors introduced in the calibration of the haploscope, experimenter mismeasurement, or any of the other systemic variables that might bias results. Notably, this error would also include refractive and tracker-based error, which we have previously analyzed (Figures 13 and 15). To attempt to quantify this error, we present a technical examination of the haploscope apparatus, where repeated measurements are taken of vergence angle mismatches, at differing IPDs and distances.

In this experiment, a calibration target (Figure 10(b)) was set up at one of five distances (33.33, 36.36, 40, 44.44, or 50 cm), and the system IPD, selected so as to span a significant percentage of the expected range of human IPDs [4], was also set to one of four distances (55, 60, 65, or 70 mm). Two cameras were set up such that both were focused straight down an optical axis of the haploscope and both showed the outer edges of the calibration glyph directly overlaid on the virtual crosshair image (Figure 17). During each trial, the experimenter had to make two adjustments: one, to rotate the wings to the appropriate angle, and the other, to adjust the bases to the appropriate IPD setting. Then, the experimenter measured the angular difference between each monitor crosshair and the center of the calibration target, and recorded the results.

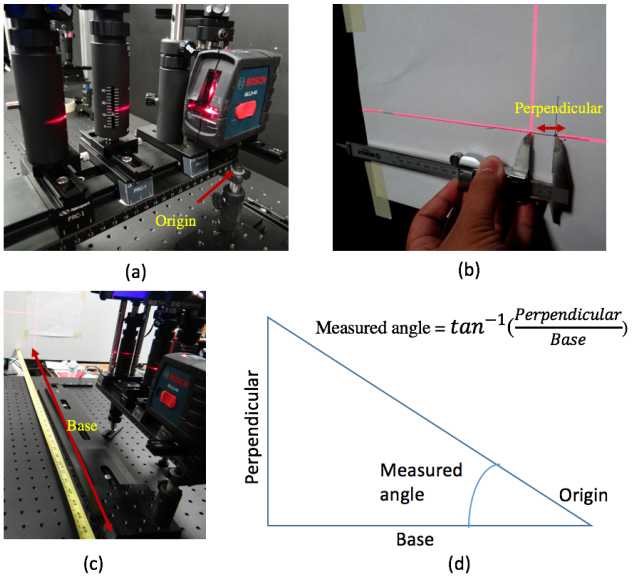

Figure 14: Experimental setup for finding angular error. (a) A laser level is positioned at the center of rotation. (b) A surface parallel to the haploscope table is used to measure the perpendicular change in position. (c) The 116 cm baseline is the distance between the origin/center of rotation and the parallel surface; having such a long baseline allows us to make very accurate angular measurements. (d) This allows us to calculate the ground truth angle of the haploscope system which can then be compared to the angle reported by the tracker.

This angular difference measure represents the amount by which our model of the haploscope is inaccurate—whether due to angular mismeasurement, experimenter error, or some other factor. Theoretically, this error should always be zero, and both sides should always have an equal angle.

In practice, of course, the results are not quite so well-behaved (Figure 16). Our observations, overall, indicate close compliance between the expected results and the actual results, particularly for smaller IPDs. Indeed, for IPD = 55 mm, the error is quite small and is explicable as a result of refraction and tracking error. However, unfortunately, the results seem to become significantly more inaccurate as the IPD increases. This, of course, warrants further analysis, particularly of IPD alignment and calibration methods, though such an analysis is currently beyond the scope of this paper.

5.4 Other Errors

It seems unlikely that the errors discussed in this section are completely exhaustive or fully representative of all errors that can be expected during haploscope calibration or use. Some of these undiscovered errors, too, may be non-systemic; they may arise from factors such as temperature variation, apparatus degradation, or nearby vibrations. Other factors, such as contrast, image quality, and color, however, may be more completely controllable. Thus, further research should be done to analyze and find potential error sources and to determine their significance.

6 Conclusions and Future Work

However, even with this important caveat, an AR haploscope remains a promising device for exploring certain perceptual questions in the context of AR systems, particularly for questions that can not be answered using current commercial hardware. While the current AR revolution may be fueled by improving availability, consumer

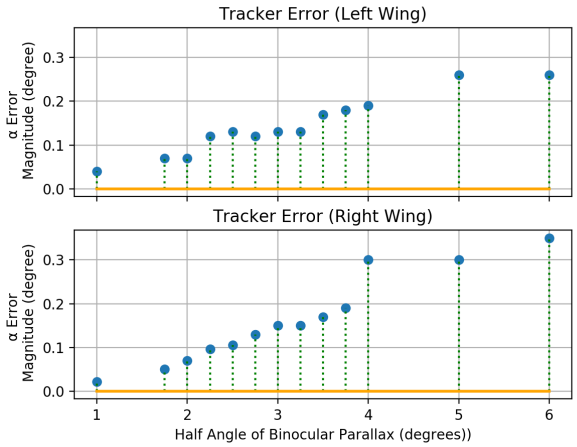

Figure 15: This graph shows the tracking error at varying distances. The x-axis represents the ostensible angle value generated by the tracker, and the y-axis represents the angular error, as tested by our triangulation method. The error increases notably as α increases (Figure 4).

confidence, and hardware, it is arguably research into these high-level perceptual issues which will provide the foundation for the longevity of the augmented reality paradigm.

Haploscope-based experiments could range from research into basic depth perception/cue interactions, to designing accommodation-invariant modalities and software, to examining the effects of visual flow on perception, to considering the relationship between cue conflicts and simulation sickness. Research like this could potentially serve to increase our understanding of the field of augmented reality and advance AR applications. Better understanding of depth perception in AR, for example, might allow the development of previously unimplementable medical applications; accommodation-invariant display technology might improve AR system performance in far-field applications; and a better understanding of simulation sickness could help improve the user experience in AR [2, 14]. These sorts of perceptual experiments would certainly make use of the novel affordances offered by haploscopes, and this research, in turn, could help support, develop, and improve the field of augmented reality.

Acknowledgments

This material is based upon work supported by the National Science Foundation, under awards IIS-0713609, IIS-1018413, and IIS-1320909, to J. E. Swan II. This work was conducted at the Institute for Neurocognitive Science and Technology, and the Center for Advanced Vehicular Systems, at Mississippi State University. We acknowledge Gurjot Singh for the initial design and calibration of the AR haploscope, and Chunya Hua for developing additional calibration methods.

References

[1] M. Banks. Visual space perception laboratory. `http://bankslab.berkeley.edu/`, 2018. Accessed: 2018-07-01.

[2] T. Cook, N. Phillips, K. Massey, A. Plopski, C. Sandor, and J. E. Swan II. User preference for sharpview-enhanced virtual text during non-fixed viewing. In *Proc. of IEEE Virtual Reality (VR)*. IEEE, March 2018.

[3] T. A. Decker, R. E. Williams, C. L. Kuether, N. D. Logar, and D. Wyman-Cornsweet. The mark iii haploscope. Technical Report NASA-CR-2584, Baylor Univ.; Dept. of Ophthalmology.; Houston, TX, United States, 1975.

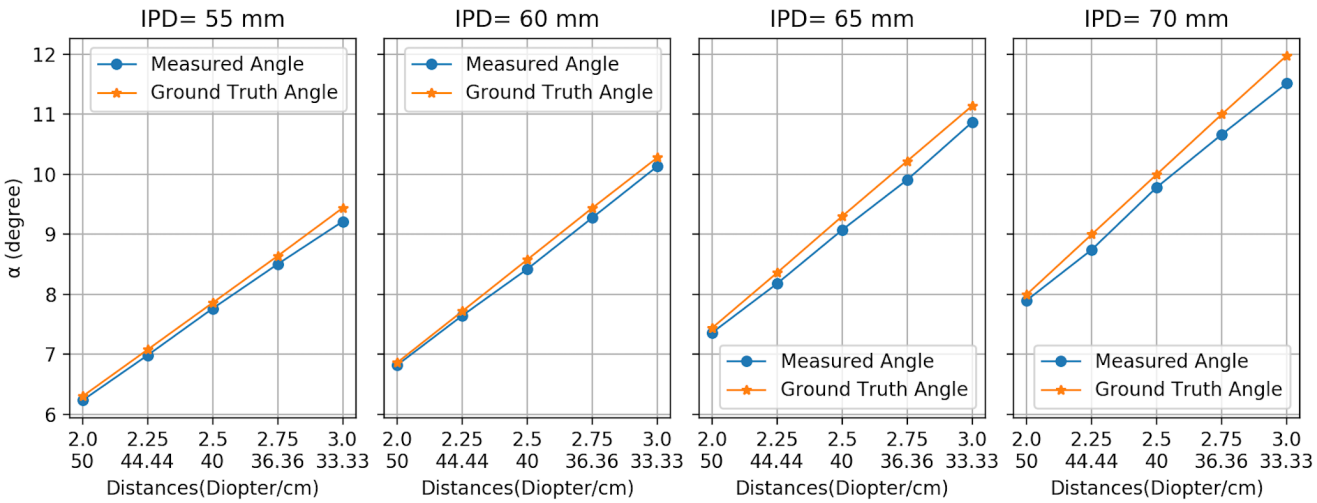

Figure 16: Results from Figure 17, showing the relationship between distance, IPD, and the angle of binocular parallax. α refers to the half angle of binocular parallax—the rotational measure the haploscope controls. The ground truth angle, calculated from Equation 1, refers to our expected result, based on our model of the haploscope and assuming complete measurement and adjustment accuracy. The measured angle is the angle that we actually observe from the system. Thus, we know that there are some error sources or inaccuracies our model does not completely account for, including those shown in Figures 13 and 15.

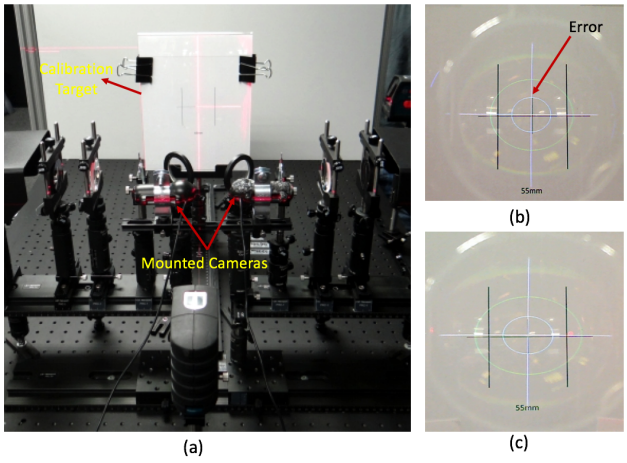

Figure 17: Experimental setup for finding angular error. (a) View of the full calibration setup, with both cameras mounted to the haploscope rail. (b) An example of a misalignment between the calibration crosshair and the monitor crosshair. (c) An example of an instance where the calibration crosshair and the monitor crosshair are perfectly aligned.

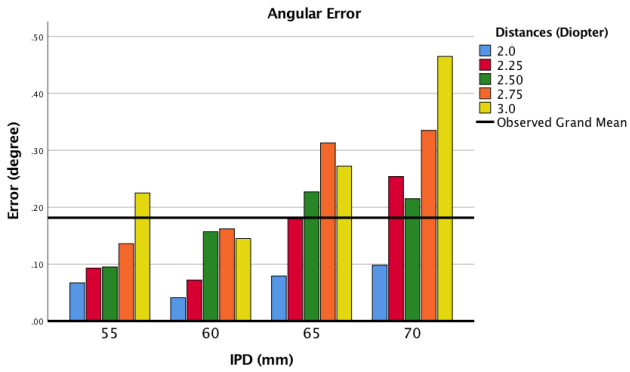

Figure 18: This bar chart shows the binocular parallax angle error across five distances and four IPDs, calculated by *error = ground truth angle − measured angle*. A positive error value indicates that the ground truth vergence angle is insufficient. As the IPD increases and distance decreases, the experimental error also increases. This is what we would expect, particularly given our tracking error results in Figure 15.

[4] N. A. Dodgson. Variation and extrema of human interpupillary distance. In A. J. Woods, J. O. Merritt, S. A. Benton, and M. T. Bolas, eds., *Stereoscopic Displays and Virtual Reality Systems XI*, vol. 5291, pp. 36–47. International Society for Optics and Photonics, May 2004. doi: 10.1117/12.529999

[5] F. Domini. 3d shape perception lab. `http://www.cog.brown.edu/research/3Dspl/research.html#cues`, 2018. Accessed: 2018-07-01.

[6] S. R. Ellis and U. J. Bucher. Distance perception of stereoscopically presented virtual objects optically superimposed on physical objects by a head-mounted see-through display. *Proceedings of the Human Factors and Ergonomics Society Annual Meeting*, 38(19):1300–1304, 1994.

[7] C. Hua. The Effect of an Occluder on the Accuracy of Depth Perception in Optical See-Through Augmented Reality. Master's thesis, Mississippi State University, Starkville, Mississippi, USA, 2014.

[8] J. A. Jones, D. Edewaard, R. A. Tyrrell, and L. F. Hodges. A schematic eye for virtual environments. In *3D User Interfaces (3DUI), 2016 IEEE Symposium on*, pp. 221–230. IEEE, 2016.

[9] E. Kruijff, J. E. Swan II, and S. Feiner. Perceptual issues in augmented reality revisited. In *Proceedings of the 9th IEEE International Symposium on Mixed and Augmented Reality 2010: Science and Technology, ISMAR 2010*, pp. 3 – 12, 11 2010.

[10] S. Lee and H. Hua. Effects of configuration of optical combiner on near-field depth perception in optical see-through head-mounted displays. *IEEE Trans. Vis. Comput. Graph.*, 22(4):1432–1441, 2016.

[11] K. Massey. Procedural Calibration of Haploscope Wings to Establish

Accurate Focal Vergence Depth. Master's thesis, Mississippi State University, Starkville, Mississippi, USA, 2018.

[12] J. Rolland, F. Biocca, F. Hamza-Lup, Y. Ha, and R. Martins. Development of head-mounted projection displays for distributed, collaborative, augmented reality applications. *Presence: Teleoperators and Virtual Environments*, 14(5):528–549, 2005.

[13] M. Shirer, T. Mainelli, and J. Ubrani. Demand for augmented reality/virtual reality headsets expected to rebound in 2018, says IDC. *International Data Corporation*, 19 March 2018. Retrieved from https://www.idc.com/getdoc.jsp?containerId=prUS43639318.

[14] G. Singh. *Near-Field Depth Perception in Optical See-Though Augmented Reality*. PhD thesis, Mississippi State University, Starkville, Mississippi, USA, 2013.

[15] G. Singh, S. R. Ellis, and J. E. Swan II. The effect of focal distance, age, and brightness on near-field augmented reality depth matching. *arXiv Preprint*, arXiv:1712.00088, Nov 2017.

[16] G. Singh, S. R. Ellis, and J. E. Swan II. The effect of focal distance, age, and brightness on near-field augmented reality depth matching. *IEEE Transactions on Visualization and Computer Graphics*, PP, Sep 2018.

[17] G. Singh, J. E. Swan II, J. A. Jones, and S. R. Ellis. Depth judgment measures and occluding surfaces in near-field augmented reality. In *Proceedings of the 7th Symposium on Applied Perception in Graphics and Visualization*, pp. 149–156. ACM, 2010.

[18] I. E. Sutherland. A Head-Mounted Three Dimensional Display. In *Proceedings of the AFIPS Fall Joint Computer Conference*, pp. 757–764. Thompson Books, 1968.

[19] J. E. Swan II, G. Singh, and S. R. Ellis. Matching and reaching depth judgments with real and augmented reality targets. *IEEE Trans. on Visualization and Computer Graphics*, 21(11):1289–1298, 2015. doi: 10.1109/TVCG.2015.2459895

[20] H. Tassinari, F. Domini, and C. Caudek. The intrinsic constraint model for stereo-motion integration. *Perception*, 37(1):79–95, 2008. PMID: 18399249. doi: 10.1068/p5501

[21] G. Westheimer. Specifying and controlling the optical image on the human retina. *Progress in Retinal and Eye Research*, 2006. doi: 10.1016/j.preteyeres.2005.05.002

[22] C. Wheatstone. On Some Remarkable, and Hitherto Unobserved, Phenomena of Binocular Vision. *Philosophical Transactions of the Royal Society of London*, 128:371–394, 1838.

[23] M. I. Williams. Haploscope. Patent US 2890620A, United States Patent Office, 1959.